AGU PUBLICATIONS

JGR

Journal of Geophysical Research: Atmospheres

RESEARCH ARTICLE

10.1002/2014JD022137

Key Points:
- We modeled the effect of Pinatubo sulfur on tropospheric photochemistry
- SO_2 absorption and aerosol extinction reduce tropospheric UV levels
- The tropospheric OH sink of CH_4 decreased by 17.8 Tg during June 1991–June 1993

Correspondence to:
N. Bândă,
n.l.banda@uu.nl

Citation:
Bândă, N., M. Krol, T. van Noije, M. van Weele, J. E. Williams, P. Le Sager, U. Niemeier, L. Thomason, and T. Röckmann (2015), The effect of stratospheric sulfur from Mount Pinatubo on tropospheric oxidizing capacity and methane, *J. Geophys. Res. Atmos.*, *120*, 1202–1220, doi:10.1002/2014JD022137.

Received 9 JUN 2014
Accepted 30 NOV 2014
Accepted article online 5 DEC 2014
Published online 12 FEB 2015

The effect of stratospheric sulfur from Mount Pinatubo on tropospheric oxidizing capacity and methane

Narcisa Bândă[1,2], Maarten Krol[1,3,4], Twan van Noije[2], Michiel van Weele[2], Jason E. Williams[2], Philippe Le Sager[2], Ulrike Niemeier[5], Larry Thomason[6], and Thomas Röckmann[1]

[1]Institute for Marine and Atmospheric Research Utrecht, Utrecht University, Utrecht, Netherlands, [2]Royal Netherlands Meteorological Institute, De Bilt, Netherlands, [3]Meteorology and Air Quality, Wageningen University and Research Center, Wageningen, Netherlands, [4]Netherlands Institute for Space Research (SRON), Utrecht, Netherlands, [5]Max Planck Institute for Meteorology, Hamburg, Germany, [6]NASA Langley Research Center, Hampton, Virginia, USA

Abstract The eruption of Mount Pinatubo in 1991 injected a large amount of SO_2 into the stratosphere, which formed sulfate aerosols. Increased scattering and absorption of UV radiation by the enhanced stratospheric SO_2 and aerosols decreased the amount of UV radiation reaching the troposphere, causing changes in tropospheric photochemistry. These changes affected the oxidizing capacity of the atmosphere and the removal rate of CH_4 in the years following the eruption. We use the three-dimensional chemistry transport model TM5 coupled to the aerosol microphysics module M7 to simulate the evolution of SO_2 and sulfate aerosols from the Pinatubo eruption. Their effect on tropospheric photolysis frequencies and concentrations of OH and CH_4 is quantified for the first time. We find that UV attenuation by stratospheric sulfur decreased the photolysis frequencies of both ozone and NO_2 by about 2% globally, decreasing global OH concentrations by a similar amount in the first 2 years after the eruption. SO_2 absorption mainly affects OH primary production by ozone photolysis, while aerosol scattering also alters OH recycling. The effect of stratospheric sulfur on global OH and CH_4 is dominated by the effect of aerosol extinction, while SO_2 absorption contributes by 12.5% to the overall effect in the first year after the eruption. The reduction in OH concentrations causes an increase in the CH_4 growth rate of 4 and 2 ppb/yr in the first and second years after the eruption, respectively, contributing 11 Tg to the 27 Tg observed CH_4 burden change in late 1991 and early 1992.

1. Introduction

The hydroxyl radical (OH) is the main oxidant in the troposphere, controlling the removal of many atmospheric pollutants [*Levy*, 1971]. The atmospheric lifetime of methane (CH_4), the second most important anthropogenic greenhouse gas, is mainly determined by OH. About 70% of CH_4 is oxidized in the tropical troposphere, where photochemistry is most active [*Lawrence et al.*, 2001]. Large uncertainties still remain about the CH_4 budget in the past decades and the role of OH in controlling CH_4 concentrations [*Kirschke et al.*, 2013; *Naik et al.*, 2013]. Chemistry and climate models [*Naik et al.*, 2013] as well as a study simulating the isotopic composition of CH_4 isotopes [*Monteil et al.*, 2011] infer a positive OH trend of up to 0.3%/yr in the past decades, while inverse modeling studies using methyl chloroform find a positive trend in OH in the 1980s, followed by a decline in the 1990s [*Krol and Lelieveld*, 2003; *Bousquet et al.*, 2005]. These studies stress that the inferred OH trend is very sensitive to uncertainties in the assumed methyl chloroform emissions. *Bousquet et al.* [2005] estimated an interannual variability (IAV) of OH between 1980 and 2000 of 8.5±1.0%. A more recent study from *Montzka et al.* [2011] finds a smaller IAV of 2.3±1.5% for the period 1998 to 2007.

The eruption of Mount Pinatubo in June 1991 caused significant global-scale radiative and climate changes which likely affected tropospheric CH_4 and OH concentrations. *Dlugokencky et al.* [1996] observed an anomalously high CH_4 growth rate during the second half of 1991, which they attributed to a decrease in the OH sink caused by changes in radiation. Subsequently, the CH_4 growth rate strongly decreased, becoming negative during late 1992, and then recovered by mid-1993 to 5 ppb/yr [*Dlugokencky et al.*, 1996].

Global-scale OH variability may be caused by variations in OH sources, sinks, and recycling between OH and HO_2, which depend on multiple factors, such as climate, and natural and anthropogenic emissions of reactants. Tropospheric OH is produced through the photolysis of ozone (O_3) by ultraviolet (UV) radiation and the subsequent reaction of $O(^1D)$ with water vapor. This primary production of OH by O_3 photolysis

in the troposphere mainly occurs at wavelengths between 290 and 330 nm. Photolysis of nitrogen dioxide (NO_2) at wavelengths up to 420 nm also affects OH concentrations because it produces nitrogen oxide (NO), important for OH recycling [*Lelieveld et al.*, 2002]. Therefore, the amount of OH in the troposphere is influenced by the amount of incoming UV radiation.

The Pinatubo eruption injected about 18.5 Tg sulfur dioxide (SO_2) into the stratosphere, which was converted to sulfate aerosols on a timescale of about 24 days [*Guo et al.*, 2004]. Having a lifetime of 1 year, sulfate aerosols remained in the atmosphere for a few years after the eruption [*Bauman et al.*, 2003]. SO_2 absorbs UV radiation between 240 and 320 nm [*Bogumil et al.*, 2003], while sulfate aerosols scatter radiation. Thus, the presence of these species in the stratosphere led to a decrease in the UV radiation entering the troposphere.

Using a box model, *Dlugokencky et al.* [1996] found the decrease in OH due to the UV attenuation by SO_2 and sulfate consistent with the high CH_4 and carbon monoxide (CO) growth rates in the second half of 1991. In their inverse modeling study, *Bousquet et al.* [2006] inferred a reduction of the OH-based sink of 26 Tg CH_4 in the 2 years following the eruption, which might be related to changes in UV radiation. Previous studies have been carried out to assess the impact of Pinatubo sulfate aerosols on shortwave and longwave radiation using 3-D chemistry climate models [e.g., *Stenchikov et al.*, 1998; *Andronova et al.*, 1999; *Timmreck et al.*, 1999]. To our knowledge, none of these studies estimated the direct effect of stratospheric sulfate on UV radiation and tropospheric photochemistry. Furthermore, studies of the Pinatubo eruption generally do not include absorption by SO_2. In the two-dimensional studies of *Bekki et al.* [1993, 1996], SO_2 absorption was shown to be important for the stratospheric ozone abundance after Pinatubo and the volcanic plume lifetime of the Toba mega-eruption.

In this study we restrict our analysis to the effects of SO_2 and sulfate described above, which are significant in the first 2 years after the eruption. The three-dimensional model TM5 is used to simulate SO_2 and sulfate aerosols from the eruption, and the corresponding changes in UV radiation, OH and CH_4 concentrations. It is important to note that changes in climate are incorporated through the use of the ERA-Interim atmospheric reanalysis from the European Centre for Medium-Range Weather Forecasts (ECMWF), and that stratospheric ozone changes are prescribed based on satellite observations. The perturbations in climate and stratospheric ozone associated with the eruption [*Bândă et al.*, 2013] will thus be included in the model runs, but their effect on the CH_4 budget is not investigated here.

The paper is organized as follows. The model setup is described in section 2. In section 3.1 we compare the modeled and observed evolution of the SO_2 and sulfate burdens. The results on tropospheric CH_4 and OH after the eruption are shown in section 3.2. The results are discussed in section 4, and conclusions are drawn in section 5.

2. Method

The atmospheric chemistry and transport model TM5 [*Huijnen et al.*, 2010; *Williams et al.*, 2012] was used in this study to simulate tropospheric photochemistry and aerosols. Aerosol microphysics is modeled by the modal scheme M7 [*Vignati et al.*, 2004; *Aan de Brugh et al.*, 2011]. In this section, the setup of the TM5 model is presented. We include a description of the changes implemented in TM5 and M7 useful for modeling volcanic SO_2 and sulfate and their effect on tropospheric chemistry. The performance of TM5 in simulating atmospheric chemistry was validated against observations in *Huijnen et al.* [2010] and *van Noije et al.* [2014], and the main conclusions of these studies remain valid under the current setup. At the end of section 2 we define the simulations performed in this study.

2.1. The TM5 Chemistry Transport Model Coupled to the M7 Aerosol Module

The TM5 model was run on 60 hybrid sigma-pressure vertical layers, at a resolution of 3°× 2° (longitude × latitude) globally, except for the polar region, where a reduced grid was used. This vertical resolution was employed because the default model configuration of 34 layers was found to produce large numerical diffusion errors for stratospheric SO_2 (see Appendix A). The model was driven by meteorological data from the ECMWF ERA-Interim reanalysis [*Dee et al.*, 2011]. The gas phase chemistry scheme is based on a modified and updated version of the carbon bond mechanism 4 [*Houweling et al.*, 1998]. The natural and anthropogenic emissions of gas phase and aerosol species used are described in Appendix B. The photolysis

frequencies were determined by the parameterization scheme based on *Williams et al.* [2006], using online radiative transfer calculation for wavelengths between 202 nm and 695 nm.

Two setups for calculating CH_4 concentrations are possible in TM5: a "free-running" setup and a "nudged" setup. In the "free-running" setup CH_4 concentrations are calculated from the balance between sources, sinks, and transport. To avoid a long-term drift in the CH_4 concentration due to small imbalances between sources and sinks, in the "nudged" setup monthly surface station data from background sites is used to constrain the CH_4 concentrations in the lowest 2 km of the model. The observed North-South gradient in CH_4 mixing ratios is obtained through latitudinal interpolation of the monthly mean observations at the stations South Pole, Cape Grim, Mauna Loa, Mace Head, Barrow, and Alert. The ratio f between the measured and modeled CH_4 mixing ratio at the dateline (0° longitude) is applied as a scaling for the modeled CH_4 in each zonal band, with a relaxation time scale of $\tau = 3$ days. The modeled CH_4 mixing ratios are then adjusted at each time step using the following equation:

$$[CH_4]_{\text{new}} = [\text{CH}_4]_{\text{old}} + [\text{CH}_4]_{\text{old}} \times (f - 1) \times (1 - e^{-\text{d}t/\tau}), \quad (1)$$

where $[\text{CH}_4]_{\text{old}}$ represents the modeled CH_4 mixing ratio, taking into account sources, sinks, and transport, $[\text{CH}_4]_{\text{new}}$ is the adjusted CH_4 mixing ratio, and dt is the time step. As will be described in section 2.2, a combination of the two setups was used in this study.

Since TM5 does not include stratospheric O_3 chemistry, O_3 is nudged to the multi sensor reanalysis data [*van der A et al.*, 2010] above 45 hPa in the tropics and above 90 hPa in the extratropics. To constrain the stratospheric loss of CH_4 by OH, Cl, and $O(^1D)$, CH_4 is also nudged above these pressure levels using climatological values from *Grooß and Russell* [2005].

The aerosol module M7 simulates the following aerosol types: sulfate (SO_4), black carbon (BC) and organic carbon (OC), sea salt, and mineral dust. In addition, TM5 simulates ammonium and nitrate using the Equilibrium Simplified Aerosol Model (EQSAM) [*Metzger et al.*, 2002], and methyl sulphonic acid. The M7 module uses seven modes to describe the size distribution of aerosols. Three modes are used for insoluble particles (Aitken, accumulation, and coarse) and four modes for soluble particles (nucleation, Aitken, accumulation, and coarse). Each mode is represented by a lognormal size distribution with a fixed width of $\sigma = 2.0$ for coarse mode particles and $\sigma = 1.59$ for the other modes.

For simulating the eruption, some adjustments were needed in this default representation of aerosols in M7. In *Kokkola et al.* [2009] the performance of the M7 scheme was tested for volcanic eruption conditions in a box model setup. They postulate that the coarse mode is representative for large sea salt and dust particles, and should not be used for modeling stratospheric sulfate, as this would lead to an overestimated particle size and to a short atmospheric lifetime of sulfate aerosol due to fast sedimentation. Furthermore, a decreased width of the particle distribution has been observed after large volcanic eruptions [*Bauman et al.*, 2003]. The findings of *Kokkola et al.* [2009] show that removing the soluble coarse mode and reducing the width of the soluble accumulation mode to σ=1.2 significantly improve the model performance in such situations. *Niemeier et al.* [2009] and *Toohey et al.* [2011] used this setup to simulate the Pinatubo eruption within the global climate model MAECHAM5-HAM, showing realistic results. We therefore use the setup recommended in *Kokkola et al.* [2009] above 300 hPa and the standard M7 setup below 300 hPa to model tropospheric aerosols. As a consequence, tropospheric coarse mode particles are restricted below 300 hPa. As stratospheric accumulation particles sediment below 300 hPa they are redistributed into the tropospheric accumulation and coarse modes. This redistribution might cause some unphysical changes in their radiative properties. However, particles have a short residence time in the troposphere of about 1 week. Therefore, we expect the error on the radiative effect of volcanic sulfate particles due to this setup to be marginal. The nucleation scheme in M7 was also adapted to handle large sulfuric acid concentrations (H_2SO_4), according to *Kokkola et al.* [2009].

To model scattering and absorption of UV radiation by aerosols interactively, the TM5 photolysis scheme has been coupled to the M7 module. Aerosol optical properties are calculated using the lookup table generated by the Generic Aerosol Optics Toolbox [*Aan de Brugh*, 2013]. Note that unlike in global climate models, the radiative transfer scheme in our model is solely used for photolysis calculation. Modeled aerosol fields are therefore coupled to the chemistry but not to the meteorological fields in our model. The perturbation in stratospheric temperature after Pinatubo is included in the reanalysis data used here through the assimilation of satellite observations.

Table 1. Setup of the Simulations

Simulation Name	Pinatubo SO_2 Emission[a]	SO_2 Absorption[b]	Pinatubo Aerosol Extinction[c]
PinS	Yes	Yes	Yes
PinS1	Yes	No	Yes
NoPinS	No	No	No

[a] SO_2 of 18.5 Tg is emitted in the model column above Mount Pinatubo (15°N 120°E), mostly between 17 and 21 km altitude during 3 h on 15 June 1991. The emitted SO_2 subsequently reacts with OH to form sulfate aerosols.

[b] SO_2 absorption is included in the radiation scheme, causing changes in photolysis frequencies.

[c] Aerosol extinction is included in the radiation scheme, causing changes in photolysis frequencies.

Absorption by SO_2 between 280 and 340 nm has been implemented in order to infer the effect of SO_2 on tropospheric photolysis frequencies. SO_2 absorption cross-section values presented in *Bogumil et al.* [2003] are used. We find the effect of SO_2 absorption on photolysis frequencies not to be significant in volcanically quiescent conditions.

2.2. Model Simulations

The simulations presented here (Table 1) were performed for the period June 1991 to May 1993, after a 1.5 year spin-up from the beginning of 1990. The spin-up was done starting from modeled concentrations of chemical species on 1 January 2007, and scaling CH_4 concentrations down by 1.5%, the ratio between observed CH_4 concentrations in 2007 and 1989. The "NoPinS" simulation corresponds to a situation without a Pinatubo stratospheric injection of sulfur. To represent the Pinatubo eruption in the "PinS" and "PinS1" simulations, an emission of 18.5 Tg SO_2 was assumed at the location of the eruption on 15 June 1991 for 3 h starting at 14.00 local time, as reported by *Wolfe and Hoblitt* [1996]. TM5 subsequently transports the SO_2 plume, and the chemistry scheme accounts for the conversion of SO_2 to sulfate particles.

The aerosol plume was observed between 19 and 24 km at the end of June 1991 at Mauna Loa station (see Figure 2a). The Microwave Limb Sounder (MLS) found peak concentrations of SO_2 at 26 km in September 1991 [*Read et al.*, 1993]. In this study the SO_2 emission was distributed vertically between 15 and 23 km, with the bulk of the emission (80%) between 17 and 21 km. Other injection heights were tested and are presented in Appendix C.

While in the PinS1 simulation only aerosols were coupled to the photolysis, in the PinS simulation both SO_2 and aerosols are allowed to interact with UV radiation. The main difference between PinS and NoPinS in the troposphere is due to the aerosol extinction of UV radiation. In the stratosphere, some additional differences in the chemistry are caused by the reaction of volcanic SO_2 with OH. The lifetime of SO_2 from Pinatubo is about 1 month, so absorption by stratospheric SO_2 becomes negligible in 1992. Therefore, PinS1 was not continued in 1992. We find the difference between PinS1 and PinS to be negligible at the end of 1991, showing that nonlinear feedbacks, such as different aerosol fields or the feedback between CH_4 and its lifetime, cause only minor changes beyond 1992. Note that the meteorological fields and stratospheric ozone values used in the three simulations have been taken from data sets that responded to the Pinatubo eruption [*van der A et al.*, 2010]. Therefore, the effects of temperature and ozone on OH and CH_4 are included in all simulations. However, differences between simulations represent only the direct effects of stratospheric sulfur.

Due to imbalances between uncertain CH_4 sources and sinks, modeled CH_4 concentrations tend to drift from observed values in free-running models. In order to account for these uncertainties, we use a two-step setup. As the first step, the PinS scenario was run with nudging to observed CH_4 concentrations, as described above. The monthly accumulated corrections introduced by the nudging to match CH_4 observations were stored. In the second step, the residual emissions (either positive or negative) obtained in the first step were used to scale the monthly CH_4 emission totals in each 10° latitude band, while maintaining the emission distribution from the original inventory. The three scenarios were run without

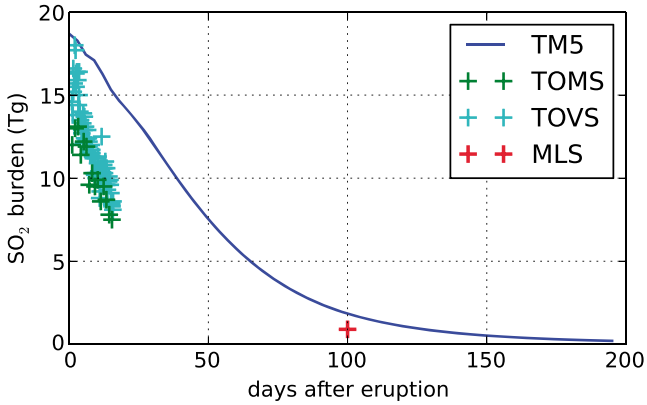

Figure 1. The modeled evolution of the stratospheric SO_2 burden and comparison with TOMS, TOVS [*Guo et al.*, 2004], and MLS estimates [*Read et al.*, 1993].

further constraining CH_4 concentrations. This setup enables us to simulate realistic CH_4 concentrations, at the same time allowing them to respond interactively to photochemical perturbations. We verified that the modeled burdens and concentrations were almost identical in the two PinS simulations. The results presented from here on are from the simulations of the second step.

3. Results

3.1. The Modeled SO_2 and Sulfate Concentrations

The evolution of the global SO_2 burden after the eruption and a comparison with estimates based on satellite observations are shown in Figure 1. Although the initial SO_2 load corresponds to the one measured by TOVS (TIROS (Television Infrared Observation Satellite) Optical Vertical Sounder) [*Guo et al.*, 2004], our model generally overestimates the stratospheric SO_2 load by about 40%. We find an SO_2 lifetime of 35 days from August to November 1991, which compares well with the estimate of 33 days based on MLS data from September 1991 [*Read et al.*, 1993]. We do not find a significant difference in the SO_2 lifetime between the PinS and PinS1 simulations. While an increase in SO_2 lifetime due to SO_2 absorption was inferred for the Toba mega-eruption [*Bekki et al.*, 1996], we do not find this to occur for Pinatubo. The initial evolution of the burden is not well captured in the model. We find a reduced loss rate in the first few days after the eruption, which may be related to OH depletion within the plume. Contrarily, TOMS (Total Ozone Mapping Spectrometer) and TOVS data indicate a shorter lifetime of 23–25 days based on measurements during the first 2 weeks after the eruption. However, we expect that the initial overestimate of the SO_2 burden and the delay of about 1 month in its conversion to sulfate does not

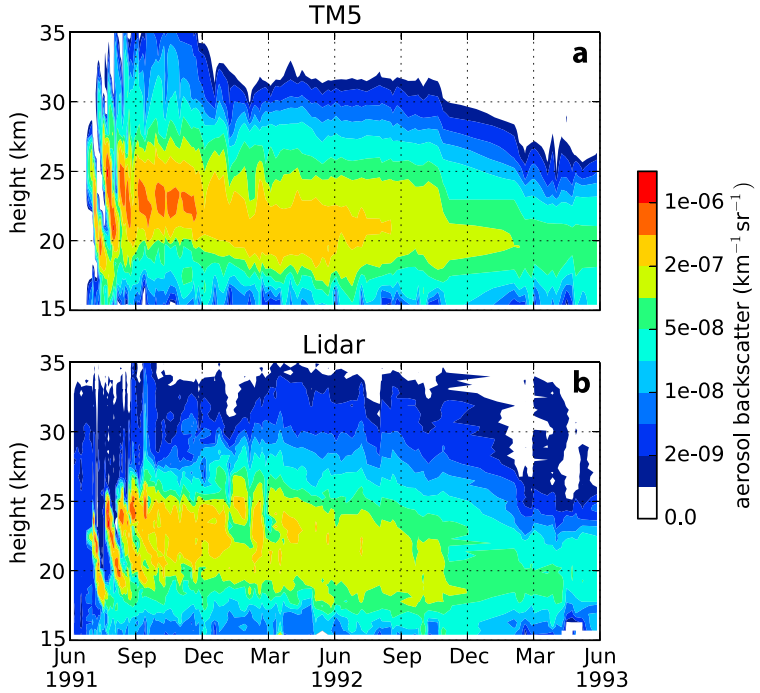

Figure 2. Evolution of (a) simulated and (b) lidar observed stratospheric aerosol backscatter profile at 694.3 nm at Mauna Loa station [*Barnes and Hofmann*, 1997] in the first 2 years after the eruption.

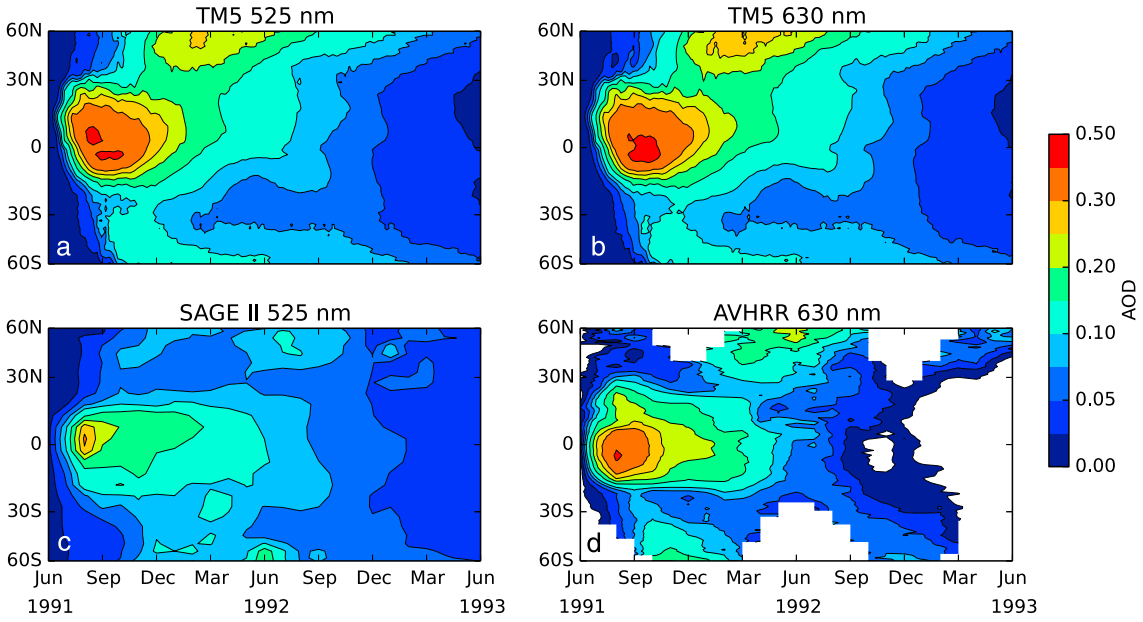

Figure 3. Evolution of the stratospheric aerosol optical depth after the eruption, modeled (a) at 525 nm and (b) at 630 nm and measured (c) by SAGE II at 525 nm [*SPARC: ASAP*, 2006] and (d) by AVHRR at 630 nm [*Zhao et al.*, 2013]. The tropospheric signal was removed from AVHRR by subtracting the AOD from 2 years prior to the eruption (June 1989 to May 1991), following the method described in *Long and Stowe* [1994]. In some areas this procedure yields negative numbers, shown here in white.

significantly affect our conclusions. The effect of the modeled SO_2 on tropospheric OH and CH_4 is found to be quite small on a global scale in comparison to the aerosol effect (see sections 3.2 and 3.3).

To investigate how well the model simulates the evolution of the stratospheric aerosol field, Figure 2 presents the modeled and measured vertical profiles of aerosol backscatter at 694.3 nm at Mauna Loa station, using observations from a ruby lidar system [*Barnes and Hofmann*, 1997]. In the first few months after the eruption, our model captures well the backscatter values below 25 km, although it overestimates the backscatter between 25 and 35 km. This overestimate might be due to the lack of reevaporation of aerosols, which becomes important near 30 km [*Dhomse et al.*, 2014]. Interestingly, periods of high backscatter occur about every 3 weeks in the first 3 months after the eruption, corresponding to the time needed for the plume to circle the globe before it is diffused in longitudinal and latitudinal directions. The agreement with observations suggests that the speed of the longitudinal transport and the latitudinal diffusion of the plume are well captured in our model. Starting from December 1991, the model agrees well with observations for both the backscatter values and the height at which the backscatter occurs.

Figure 3 shows the evolution of the zonal averaged aerosol optical depth (AOD) observed by SAGE II (Stratospheric Aerosol and Gas Experiment II) [*Stratospheric Processes and their Role in Climate (SPARC): Assessment of Stratospheric Aerosol Properties (ASAP)*, 2006; *Thomason et al.*, 2008] at 525 nm above 10 km by AVHRR (Advanced Very High Resolution Radiometer, data version 2.0) [*Zhao et al.*, 2013] at 630 nm, and the corresponding modeled values. Since AVHRR measures the total column AOD including the troposphere, we removed the tropospheric signal by subtracting the AVHRR-measured AOD from the 2 years before the eruption (June 1989 to May 1991), as described in *Long and Stowe* [1994]. The modeled AOD at 525 nm is generally lower than that at 630 nm. Since the simulated volcanic particles grow to 0.42 μm (Figure 4), they have a peak extinction efficiency around 0.6 μm. This wavelength dependence of the AOD was also captured by SAGE II, which showed highest extinction values for 525 nm among the four measured wavelengths (386, 452, 525, and 1020 nm) during 1992 and 1993 [*Bauman et al.*, 2003]. The AOD values in our model are generally higher than those measured by SAGE II and AVHRR in the tropics and northern midlatitudes in the first year after the eruption. AOD reaches 0.45 in the tropics in autumn 1991, higher than the observed values of less than 0.35 by SAGE II and less than 0.4 by AVHRR. The transport of the volcanic cloud to both Northern and Southern Hemispheres is captured reasonably well by the model. However, the transport to the northern high-latitudes is more pronounced in the model compared to

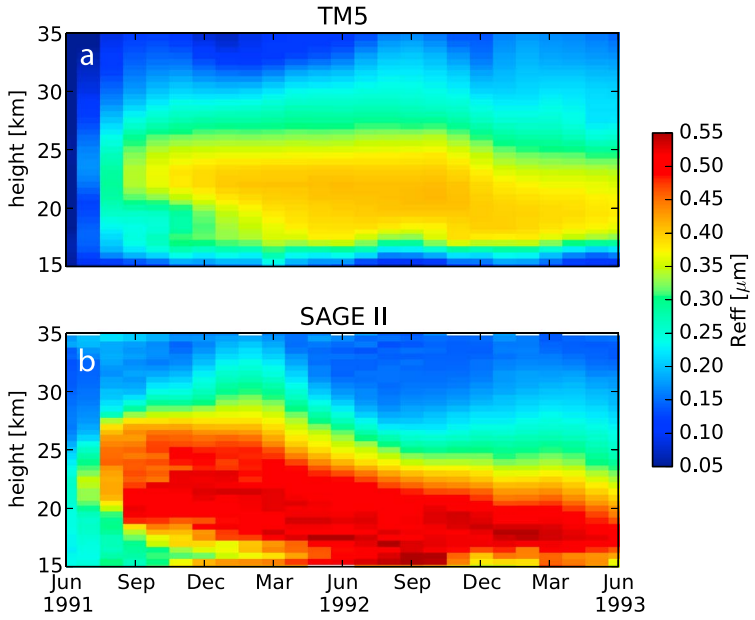

Figure 4. Evolution of the mean aerosol effective radius profile in the 10–20°N latitude band, (a) modeled and (b) measured by SAGE II [*ASAP*, 2006].

observations, while the transport to the southern high-latitudes is less pronounced than in the SAGE II data. In the second year after the eruption the modeled AOD compares well to SAGE II data and is about 0.05 lower than the AVHRR data. In Appendix C we show that the AOD match with observations deteriorates when a different emission height is chosen. Concerning the lifetime of the Pinatubo aerosols, we find a value of 1.23 years, which is in the range of 1–1.37 years estimated based on lidar data at tropical and midlatitude stations [*Barnes and Hofmann*, 1997; *Nagai et al.*, 2010; *Deshler*, 2008].

The modeled aerosol effective radius between 10° and 20°N reaches a maximum of 0.42 μm, while the SAGE II estimate reaches 0.55 μm (Figure 4). The height of the aerosol layer is reasonably well estimated, with an upper bound around 27–30 km. The modeled effective radius is within the uncertainties of the measured effective radius from SAGE II, which give a lower estimate of 0.4 μm [*Bauman et al.*, 2003]. It also falls within the lower range of the lidar observations performed in northern Germany [*Ansmann et al.*, 1996]. Potential underestimations in aerosol size might be due to the use of parametrized water uptake on aerosols from *Zeleznik* [1991], as in the original M7 scheme, which underestimates the uptake under stratospheric conditions [*Carslaw et al.*, 1995]. Another possible reason is the model resolution, which dilutes areas with large concentrations of aerosols, decreasing aerosol coagulation in the first months after the eruption (see Appendix A). Our initial simulation on 34 vertical layers instead of 60 compared much poorer to the backscatter and AOD observations, with aerosol effective radius reaching only 0.28 μm. This indicates that the obtained results are quite sensitive to the model resolution.

3.2. Changes in OH and *J* Values

Figure 5 shows the time evolution of the zonal mean tropospheric *J* values and OH concentrations, and differences between the three simulations. The tropopause was defined as a function of latitude as recommended in *Lawrence et al.* [2001], and the vertical averaging was done by weighting with the air mass. The strongest reductions in J_{O_3} occur in the tropics (Figure 5d), where decreases of more than 10^{-6} s^{-1} between NoPinS and PinS are found from June to September 1991. The decrease in the photolysis frequency of NO_2 (J_{NO_2}, Figure 5e) is weaker in the tropics, reaching 0.15×10^{-3} s^{-1} in autumn 1991, and more significant at midlatitudes, with reductions of more than 0.25×10^{-3} s^{-1} in the northern midlatitudes from November 1991 to April 1992. The stronger decrease in J_{NO_2} at midlatitudes is related to a larger solar zenith angle. J_{NO_2} depends more strongly on direct radiation than J_{O_3}, which depends more strongly on diffuse radiation. With increasing solar zenith angle, the path of direct sunlight through the aerosol layer is longer, and therefore, the amount of direct radiation is more strongly attenuated. The resulting change in OH,

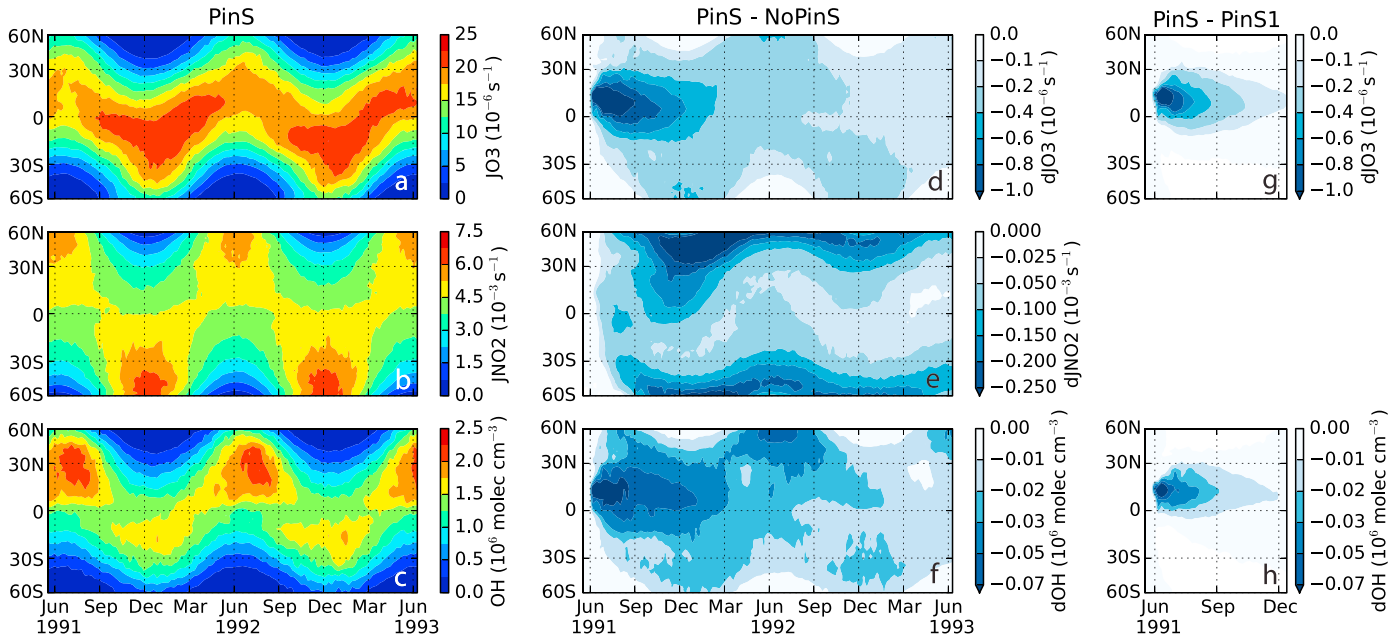

Figure 5. Evolution of the zonal mean tropospheric (a) J_{O_3}, (b) J_{NO_2}, and (c) OH, and differences (d–f) between the PinS and NoPinS simulations, and (g and h) between the PinS and PinS1 simulations. For the difference PinS-PinS1, only the first 6 months are shown. The difference in J_{NO_2} between PinS and PinS1 is omitted because it is found to be negligible.

shown in Figure 5f, is a decrease of more than 3×10^4 molec cm^{-3} at 0–30°N from July 1991 to March 1992, and at 30–60°N during the summer of 1992.

By taking the difference between the results of the PinS and the PinS1 simulation, we find the effect of the SO_2 absorption on UV radiation. In the first week after the eruption, the total column SO_2 amounts to more than 150 Dobson Units (DU) above Eastern Africa and the Indian Ocean (not shown), leading to decreases of more than 50% in J_{O_3} and more than 35% in OH in the troposphere. This strong effect is quite localized, lasting for only a few weeks, and is less important on a global scale. This can be seen in Figures 5g and 5h, where the zonal mean effect of SO_2 absorption on tropospheric OH and J_{O_3} is plotted. Since SO_2 does not absorb at wavelengths larger than about 320 nm, at which NO_2 photolysis takes place predominantly, J_{NO_2} is mostly unaffected and therefore not shown here. The effect of SO_2 absorption is restricted to the northern tropical region, with maximum decreases in the zonally averaged J_{O_3} and OH of 0.8×10^{-6} s^{-1} and 4×10^4 molec cm^{-3}, respectively, during the first month after the eruption. With the SO_2 being converted almost entirely to aerosol within 3 months, its zonal mean effect on J_{O_3} and OH decreases to less than 0.3×10^{-6} s^{-1} and 2×10^4 molec cm^{-3}, respectively, by September 1991.

Figure 6 shows the evolution of the relative changes in the global mean vertical profiles of J_{O_3}, J_{NO_2}, and OH between the three simulations. Extinction of UV radiation by sulfate aerosols and absorption by SO_2 lead to decreases in J_{O_3}, J_{NO_2}, and OH below the volcanic plume between the NoPinS and PinS simulations (Figures 6b–6d). The photolysis frequencies and OH concentrations between 25 and 35 km increase by up to 2% due to an increase in UV radiation in the upper part of the aerosol plume and above. OH and J values are affected by aerosol extinction throughout the atmosphere for 2 years after the eruption, with decreases of more than 2% in OH until the end of 1992. The decrease in J_{O_3} intensifies near the surface, while J_{NO_2} is affected more in the upper troposphere. As a result, OH decreases throughout the troposphere. At altitudes between 15 and 25 km, global mean OH decreases by 5–10% during the first 2 months after the eruption as a result of OH destruction within the plume by the reaction with SO_2. The SO_2 absorption affects O_3 photolysis throughout the column below the volcanic cloud, as can be seen in Figure 6f. The effect on tropospheric OH is a 1% decrease in the troposphere shortly after the eruption and gradually diminishes afterward. This effect is about half of the relative effect of SO_2 absorption on J_{O_3}.

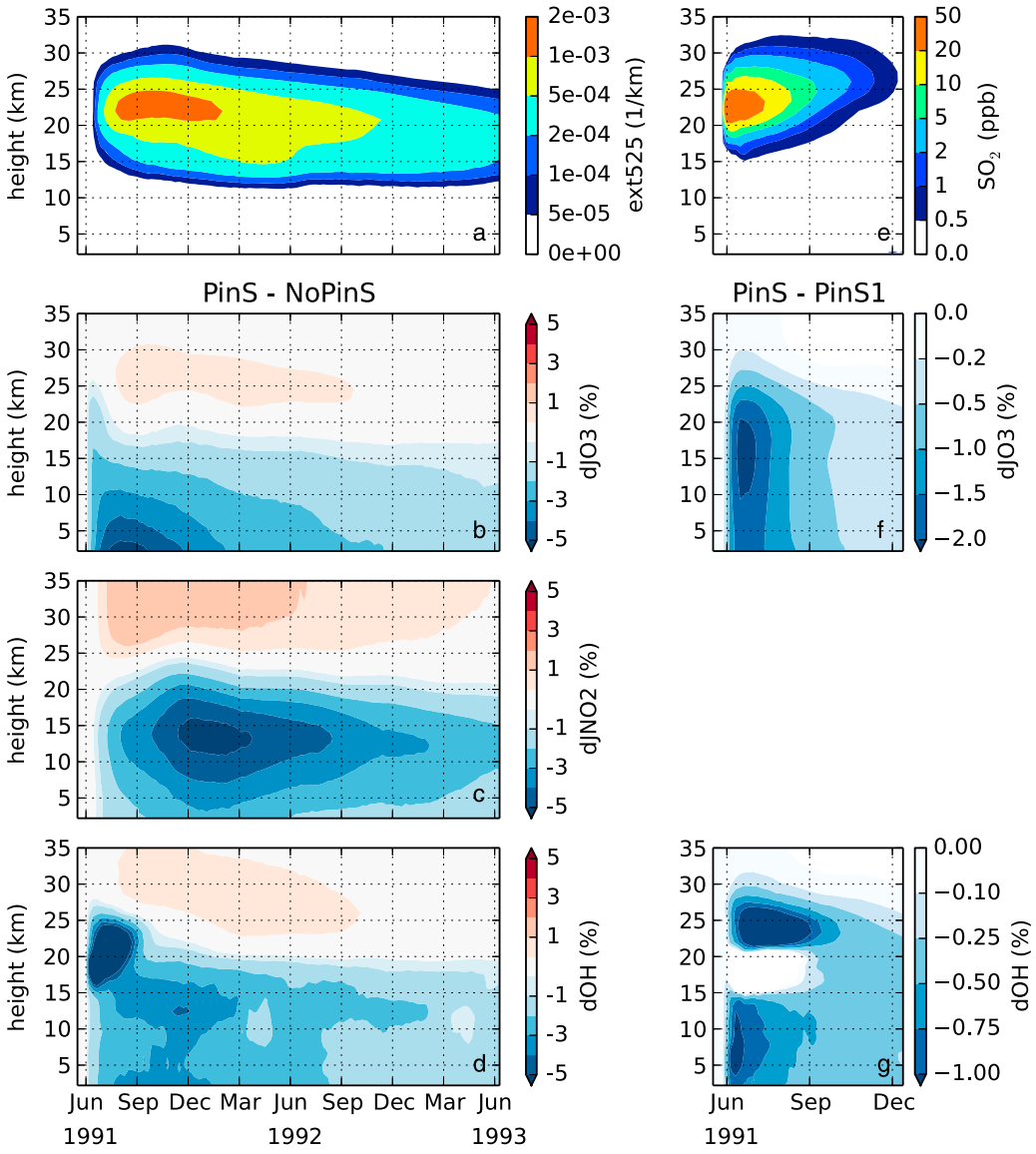

Figure 6. Evolution of the differences in the global mean profile of tropospheric J_{O_3}, J_{NO_2}, and OH between the (b–d) PinS and NoPinS simulations, and between the (f and g) PinS and PinS1 simulations. The global mean profiles of (a) extinction at 525 nm and (e) SO_2 concentrations are also shown.

3.3. CH_4 After Pinatubo

Table 2 lists the chemical budget terms of CH_4 and O_3, and lifetimes of CH_4, O_3, and CO affected by the change in UV radiation due to volcanic SO_2 and aerosols. Global budget values are shown for the PinS simulation, as well as the absolute changes in the budget terms for the other two simulations. The loss of O_3 through photolysis decreases by 47.4 Tg (2.2%) in the first year and by 23.7 Tg (1.1%) in the second year after the eruption due to Pinatubo SO_2 and aerosols. Decreases are also found in the chemical production of O_3 from the reactions of NO with HO_2 and RO_2, and in the loss of O_3 through the reactions with OH and HO_2. These effects nearly cancel out, leading to changes in the O_3 burden of less than 1 Tg each year. The modeled CH_4 lifetime is 8.8 and 8.7 years in the first and second years after the eruption, in good agreement with the observation-based present-day estimate of 9.1±0.9 years [*Prather et al.*, 2012] and with the multimodel mean lifetime of 8.6±1.2 years from the Atmospheric Chemistry and Climate Model Intercomparison Project (ACCMIP) [*Voulgarakis et al.*, 2013]. Since both CH_4 and CO are destroyed by OH, their lifetimes increase between the NoPinS and PinS simulations. We find increases in the CH_4 lifetime by

Table 2. Global Yearly Budgets and Differences Between Budget Terms Between the Three Simulations[a]

	PinS First year[c]	ΔPinS[b] First Year[c]	ΔPinS1[b] First Year[c]	PinS Second Year[c]	ΔPinS[b] Second Year[c]
CH_4 emissions[d]-soil sink	520.8	-	-	508.1	-
CH_4+OH troposphere	464.2	−11.2	−9.8	468.1	−6.6
CH_4 stratospheric loss	36.1	−0.2	−0.3	36.1	−0.9
CH_4 burden change	20.5	11.0	9.5	3.9	5.5
NOAA CH_4 burden change	27.2			2.9	
Tropospheric O_3 chemical production	4415.7	−57.2	−50.2	4489.7	−32.4
Tropospheric O_3+hν	2171.9	−47.4	−39.6	2198.4	−23.7
Tropospheric O_3 other chemical losses	1826.4	−11.9	−12.1	1853.4	−9.2
Tropospheric O_3 burden change	−2.0	1.0	1.2	−5.1	−0.2
CH_4 lifetime[e] (years)	8.8	0.2	0.2	8.7	0.1
CO lifetime[e] (days)	55.1	1.5	1.4	54.0	1.0
Tropospheric O_3 lifetime[e] (days)	30.1	0.4	0.4	29.0	0.2

[a]Global yearly budgets are shown for the simulation with Pinatubo and absolute differences for PinS and PinS1 with respect to NoPinS in the first and second years after the eruption. For O_3, only tropospheric budget terms are shown, with the tropopause defined as in *Lawrence et al.* [2001]. Numbers are in teragram unless otherwise specified.

[b]ΔPinS = PinS − NoPinS; ΔPinS1 = PinS1 − NoPinS.

[c]First and second years after the eruption are defined as 1 June 1991 to 31 May 1992, and 1 June 1992 to 31 May 1993, respectively.

[d]Note that CH_4 global emissions have been scaled with the nudging term determined by the model in a previous simulation with CH_4 constrained to observations (see section 2.2).

[e]Lifetimes were calculated as the ratio between the atmospheric burden and the total loss.

0.2 year (2.2%) in the first year and 0.1 year (1.4%) in the second year. The CO lifetime increases by 1.5 days (2.7%) in the first year and 1 day (1.9%) in the second year. A small part of this increase in the first year is related to the absorption of UV radiation by SO_2.

The CH_4 burden change during 1991 and 1992 can be estimated using global mean CH_4 mixing ratios from NOAA [*GLOBALVIEW-CH4*, 2009]. The ratio of 2.78 Tg/ppb reported by the Intergovernmental Panel on Climate Change (IPCC) [*Denman et al.*, 2007] was used to convert from observed surface CH_4 mixing ratio to CH_4 burden. In 1991 the burden change obtained using this approach amounts to 27.2 Tg, while in 1992 an increase of only 2.9 Tg was observed. We model a CH_4 burden change of 20.5 Tg over the coarse of the first year after the eruption, when accounting for the radiative effects of stratospheric sulfur from Pinatubo (PinS) and nudging the methane concentrations with surface observations. More than half of the modeled increase in CH_4 burden, 11 Tg, is related to the decrease in the OH sink of CH_4 due to stratospheric sulfur from the Pinatubo eruption. During the second year after the eruption, we find an increase of 3.9 Tg in the CH_4 burden in the PinS simulation, while stratospheric sulfur leads to an increase of 5.5 Tg. Therefore, we find a decrease of 1.6 Tg in the CH_4 burden in the NoPin simulation. The differences of 6.7 Tg and 1.0 Tg between the NOAA-based and modeled burden changes in 2 years after the eruption may be due to the larger set of stations used in GLOBALVIEW-CH4 compared to the set used to constrain our model (section 2.1). Furthermore, additional processing steps have been performed to homogenize the GLOBALVIEW-CH4 data. By employing the ratio of 2.78 Tg/ppb CH_4, we find that stratospheric sulfur from Pinatubo leads to an increase in the methane growth rate of 4.0 and 2.0 ppb/yr in the first and second years after the eruption, respectively. In the first year, the SO_2 absorption accounts for 0.5 ppb/yr of this increase, contributing by 12.5% to the overall effect.

Differences in the CH_4 removal by OH in the global troposphere between the three simulations are presented in Figures 7a and 7c. The latitudinal distribution of these changes are shown in Figures 7b and 7d. SO_2 absorption leads to a small reduction of the CH_4 sink in the tropics during the first few months after

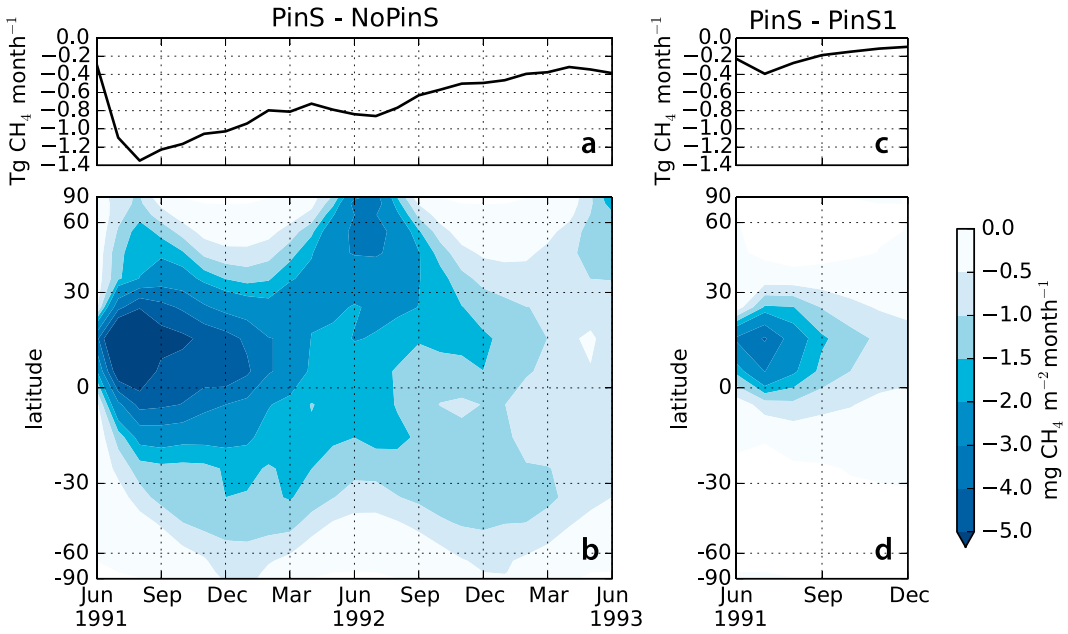

Figure 7. (a) Differences in the global tropospheric OH sink of CH_4 and (b) differences in the latitudinal average sink strength, integrated over the tropospheric column between the PinS and NoPinS simulations; (c and d) corresponding differences between the PinS and PinS1 simulations.

the eruption, leading to an increase in the CH_4 burden of 1.4 Tg globally. The aerosol extinction determines more significant changes both in the tropics and during summer in the extratropics. Overall, we find global decreases in the tropospheric CH_4 sink due to volcanic stratospheric sulfur of 11.2 Tg and 6.6 Tg during the first year and the second year after Pinatubo, respectively.

4. Discussion

Several results presented above require additional analysis. First, the relative effect of SO_2 absorption on tropospheric OH is about half the relative effect on J_{O_3}. *Fuglestvedt et al.* [1994] find a ratio of 1.6, between the relative change in tropospheric J_{O_3} and the relative change in OH due to stratospheric ozone changes, using a steady state assumption representative for the year 1990. Assuming an equilibrium between the production of OH from photolysis and the main losses of HO_X (HO_2+HO_2 and HO_2+OH), they derive the relation $P = \beta \times [OH]^2$, with P the production rate of OH and β a factor that depends on the ratio $[OH]/[HO_2]$. If β is constant, this implies a relation between a small change in OH production (ΔP) and a small change in OH ($\Delta[OH]$) that satisfies $\Delta P = 2\beta \times \Delta[OH] \times [OH]$. The associated relative change in P is twice the relative change in OH ($\Delta P/P = 2\Delta[OH]/[OH]$). This relation is satisfied in our model, where the local and short-term changes in UV radiation due to SO_2 absorption only marginally affect concentrations of CO and NO_X, which drive the recycling between OH and HO_2 and determine β. In the case of *Fuglestvedt et al.* [1994], the effect is global and long term, so the relationship is slightly changed. We find relative changes in J_{O_3}, J_{NO_2}, and OH due to sulfate aerosols of similar magnitude, showing that in this case not only the primary production of OH is affected but also the OH recycling and the ratio between OH and HO_2.

Another aspect that deserves attention is the vertical distribution of the effect on photolysis frequencies. We presented in Figure 6 the relative change in photolysis frequencies due to Pinatubo aerosols. While the effect on O_3 photolysis maximizes near the surface, the effect on J_{NO_2} maximizes in the upper troposphere. This can be explained by analyzing the contributions of direct and diffuse radiation at different wavelengths and how they are affected by the aerosol layer. The primary response to a stratospheric aerosol layer is a decrease in the direct radiation and an increase in the diffuse radiation in the troposphere. While the effect on direct radiation is relatively constant with height, the aerosol layer increases more efficiently the diffuse radiation in the upper troposphere. This is because of the strong Rayleigh scattering in the lower troposphere, even in the absence of aerosols. By analyzing the relative contributions to diffuse

and direct radiation, we found that the net effect on radiation depends in a complex way on height, wavelength, and solar zenith angle. Most O_3 photolysis in the troposphere occurs at small solar zenith angles, at a wavelength of about 300 nm, when direct and diffuse radiation contribute in similar amounts to the total radiation. In this case, the stratospheric aerosol layer causes a decrease in total radiation, due to a decrease in direct radiation, which is counteracted near the tropopause by an increase in diffuse radiation. At 400 nm, where NO_2 photolysis predominantly occurs, molecular scattering is less efficient. Therefore, in the upper troposphere the total radiation is dominated by the direct radiation, while the diffuse radiation is more important near the surface. This causes the relative decrease in total radiation at 400 nm to be more pronounced near the tropopause.

Previous attempts to quantify the effect of volcanic SO_2 from Pinatubo on CH_4 have been made using column models. Although they are useful for illustrating the processes involved, an accurate regional or even global estimate of this effect using a column model is difficult due to the localized nature of the SO_2 plume. *Dlugokencky et al.* [1996] found a 12% decrease in J_{O_3} in the 9°S–9°N equatorial band, and *Bândă et al.* [2013] estimated a global 2.5% reduction in OH immediately after the eruption. In our simulations, SO_2 absorption leads to a maximum decrease of 1% in the global tropospheric OH and up to 3% in the northern tropical band. The above studies probably overestimate the effect of SO_2 by assuming an instant homogeneity of the SO_2 plume in the equatorial band or around the globe, due to the nonlinearity of the atmospheric photochemistry. In the present study we are able to take this into account more precisely by simulating the dispersion of the SO_2 plume. However, we might also overestimate this effect due to the large stratospheric SO_2 burden compared to observations.

The effect of aerosol extinction found by *Dlugokencky et al.* [1996], i.e., a maximum 6% reduction in J_{O_3} in the band 9°S–9°N, is similar to our findings. However, we also find significant effects on J_{NO_2}, and on J_{O_3} outside of this equatorial band, which are important for the global OH sink of CH_4. *Bândă et al.* [2013] found a maximum global increase in the CH_4 growth rate of 3.5 ppb/yr due to Pinatubo aerosols, while this study finds a maximum change of 1.35 Tg in August 1991 in the OH sink, equivalent to a growth rate increase of 5.8 ppb/yr. In their study, global mean AOD values were used, assuming aerosols to be evenly distributed around the globe. However, most CH_4 is destroyed in the tropical troposphere, where stratospheric AOD values exceed 0.4.

Using an inverse modeling approach, *Bousquet et al.* [2006] estimated a decrease in the tropospheric OH sink of CH_4 during 1991–1993 compared to the 1984–2003 mean of 26 Tg or 8.7 Tg/yr. This is very similar to our estimate of 17.8 Tg in 2 years or 8.9 Tg/yr on average. However, in our case we isolate the effect of aerosols and SO_2, while the OH fields used in *Bousquet et al.* [2006] were derived from inverse modeling of methyl chloroform. These fields also respond to other forcings after the eruption, such as changes in water vapor and stratospheric ozone, which might contribute to their estimated change in the tropospheric OH sink of CH_4. The good agreement between our result and *Bousquet et al.* [2006] suggests that other effects on OH in this period compensate each other, which was also shown to partly occur in *Bândă et al.* [2013].

There has been a debate on the magnitude of the global OH interannual variability (IAV). Previous studies estimated an IAV of 7–9% [*Bousquet et al.*, 2005; *Prinn et al.*, 2005]. However, as argued by *Montzka et al.* [2011], these estimates were likely affected by uncertainties in methyl chloroform emissions. Based on the decline of methyl chloroform since 1998, *Montzka et al.* [2011] derived a lower IAV in OH of 2.3±1.5%. Our calculated response of tropospheric OH to the Pinatubo eruption (a reduction of about 2%) is in line with this finding.

Although our approach in quantifying the effects of stratospheric sulfur from Pinatubo on tropospheric chemistry is more sophisticated than previous attempts, our estimate still contains some uncertainty related to the modeled SO_2 and sulfate load. Our model overestimates by about 40% the stratospheric SO_2 burden due to an overestimate in the SO_2 lifetime in the first month after the eruption, in particular not capturing the reduced lifetime in the first few days after the eruption. *Guo et al.* [2004] suggest that catalytic reactions on ice and ash particles enhanced the SO_2 removal in the first few days after the eruption, with about 3 Tg SO_2 being converted to sulfate within the eruption column. Such processes are not included in our model. Model resolution can also affect nonlinear chemical processes in the early stage of the plume. Another possible reason for the initially enhanced SO_2 lifetime in the model compared to observations may be related to uncertainties in the modeled OH in the lower stratosphere due to missing stratospheric chemistry, or due to uncertainties in stratospheric water vapor fields [*Oikonomou and O'Neill*, 2006].

Enhanced OH concentrations were observed in the stratosphere after the eruption of El Chichon [*Burnett and Burnett*, 1984] and were attributed to water vapor emission from the eruption. A large water vapor increase from the Pinatubo eruption would not be well captured in the ERA-Interim data used in our simulations.

The modeled aerosol distributions also show some discrepancies with satellite observations, with overestimated AOD in the tropics and at high latitudes in the Northern Hemisphere in the first year after the eruption. These features are also found in other studies that simulate the Pinatubo aerosols using general circulation models [*Niemeier et al.*, 2009; *Aquila et al.*, 2012; *English et al.*, 2013; *Dhomse et al.*, 2014]. Some differences between modeled and observed AOD might be related to measurement uncertainties. AVHRR measures the total AOD in nadir view, which makes it difficult to distinguish the stratospheric and the tropospheric contributions. SAGE II measures the vertical profile of aerosol extinction in limb view and is generally taken as a reference for global climate studies. In the first year after the eruption, the SAGE II instrument was saturated, and the data used here have been gap-filled based on surface lidar data [*SPARC: ASAP*, 2006]. The more reliable SAGE II data from the second year after the eruption are well represented by the model. Aerosol backscatter at the tropical station Mauna Loa is generally well captured, but also suggest an overestimate of the simulated stratospheric aerosol burden in the tropical band in the first months after the eruption.

The modeled transport of the aerosol plume to the Northern Hemisphere is more pronounced than to the Southern Hemisphere, while observations show an equally pronounced transport to the two hemispheres. The observed aerosol load in the Southern high latitudes might be partly related to the eruption of Cerro Hudson in August 1991. This additional eruption, which injected 1.5 Tg SO_2 in the stratosphere at 45°S [*Doiron et al.*, 1991], is not included in our model simulation. Other uncertainties in the latitudinal distribution of the plume might be related to uncertainties in transport. The cross-equatorial transport of the Pinatubo plume was shown to be a result of dynamical changes caused by the absorption of longwave radiation by sulfate aerosols in the first 2 weeks after the eruption. The coupling between radiation and aerosols proved to be essential for simulating the southern transport of the Pinatubo plume in studies using global climate models [*Young et al.*, 1994; *Timmreck and Graf*, 2006; *Aquila et al.*, 2012]. Our model is driven by reanalysis winds, which are not coupled to the aerosol fields simulated by TM5. Furthermore, the aerosols from Pinatubo are not explicitly included in the ECMWF model. However, their effect on stratospheric temperatures is accounted for by assimilating satellite observations. Indeed, the long-term trend in stratospheric temperature after Pinatubo is well captured in ERA-Interim, with a 15% attenuation of the observed volcanic signal [*Dee et al.*, 2011]. However, more localized effects, such as the effect of aerosol absorption on stratospheric dynamics in the first 2 weeks after the eruption, are probably not well represented due to scarcity of observational data available for assimilation in the ECMWF model.

Based on the uncertainties in modeled SO_2 burden, aerosol load, and aerosol size, we roughly estimate a 15% uncertainty in the modeled effect of stratospheric sulfur on the CH_4 burden in the first 2 years after the eruption.

5. Conclusions

We quantified for the first time the effect of SO_2 and sulfate aerosols from the Pinatubo eruption on tropospheric photochemistry using a three-dimensional global chemistry model. The overall impact of decreased UV radiation due to stratospheric sulfur on CH_4 during the first 2 years after the eruption was a decrease of 17.8 Tg in the CH_4 sink. This decrease was dominated by the effect of UV radiation scattering by volcanic aerosols. Stratospheric SO_2 absorption caused a reduction of 1.4 Tg in the CH_4 sink in the first few months after the eruption.

Due to the Pinatubo stratospheric sulfur, the global CH_4 growth rate was increased by 4.0 ppb/yr and 2.0 ppb/yr in the first and second year after the eruption, respectively. Based on the observed growth rate of CH_4 concentrations, the burden change of CH_4 in the first year after the eruption is estimated to be about +27 Tg. The calculated effect of sulfur from Pinatubo in our simulation amounts to a burden change of +11 Tg in the same period. Therefore, the reduction in OH from the enhanced SO_2 and aerosol can explain about 40% of the observed CH_4 burden change in the period June 1991 to May 1992. In the second year after the eruption, the observed CH_4 burden change is +2.9 and the simulated sulfur effect is +5.5 Tg. This

suggests that other processes counteracted this reduction of the chemical sink due to stratospheric sulfur in the second year, for example, decreasing emissions or other factors affecting the sink.

This article investigates solely the direct effect of stratospheric sulfur on UV radiation and the related effects on the tropospheric OH sink of CH_4. Although we show that the sulfur emissions from Pinatubo play a significant role in the methane budget, the exact reasons for the observed decrease in the CH_4 growth rate in 1992 remain unresolved. Several processes have been proposed to explain these observations, including an increase in the tropospheric OH sink due to stratospheric ozone depletion on sulfate aerosols [*Telford et al.*, 2009; *Bekki et al.*, 1994; *Wang et al.*, 2004; *Bândă et al.*, 2013], decreased emissions from wetlands due to lower temperatures [*Dutton and Christy*, 1992; *Bekki and Law*, 1997; *Walter et al.*, 2001; *Bândă et al.*, 2013], and decreased anthropogenic emissions due to the collapse of the Soviet Union [*Dlugokencky et al.*, 1994]. These effects are included in our simulations, by imposing realistic year-to-year variations in meteorology, stratospheric ozone, and CH_4 emissions. Their impact on tropospheric chemistry will be assessed in a future study.

Appendix A: Sensitivity to Vertical Resolution

The standard TM5 model setup uses 34 vertical layers out of the 60 sigma hybrid sigma-pressure vertical layers of ERA-Interim. This setup has a resolution of 4–5 km in the stratosphere above 23 km, while the full 60 layers of ERA-Interim have a resolution of 2 km or less up to 45 km altitude. Figure A1 shows a comparison between the mean SO_2 profile over the 20°S–20°N latitude band for two simulations performed using 34 and 60 layers, respectively. The 34 layer version of the model transports SO_2 to the top of the model domain at 55 km altitude within a couple of weeks. Concentrations of more than 1 ppb of SO_2 are found at this altitude between August and November 1991. When using 60 layers, most of the SO_2 remains below 40 km throughout the simulation, with mean zonal concentrations over 1 ppb only between 15 and 33 km. We conclude that the slopes advection scheme [*Russell and Lerner*, 1981], which is default in TM5, is not able to resolve the large SO_2 gradients in the stratosphere on a 5 km resolution. The resolution also affects the aerosol concentrations, with aerosols being formed in the 34 layer version up to 55 km. The aerosol plume is more diluted, leading to less coagulation and smaller aerosol size of 0.28 nm (not shown), much smaller than the observations (Figure 4). Therefore, we chose to use the full 60 layer configuration for the simulations presented in this paper. To check whether the model continues to be diffusive on 60 layers, an additional simulation was performed using the second moment of the advection scheme [*Prather*, 1986]. However, this did not lead to any significant further difference in the modeled stratospheric aerosol or SO_2.

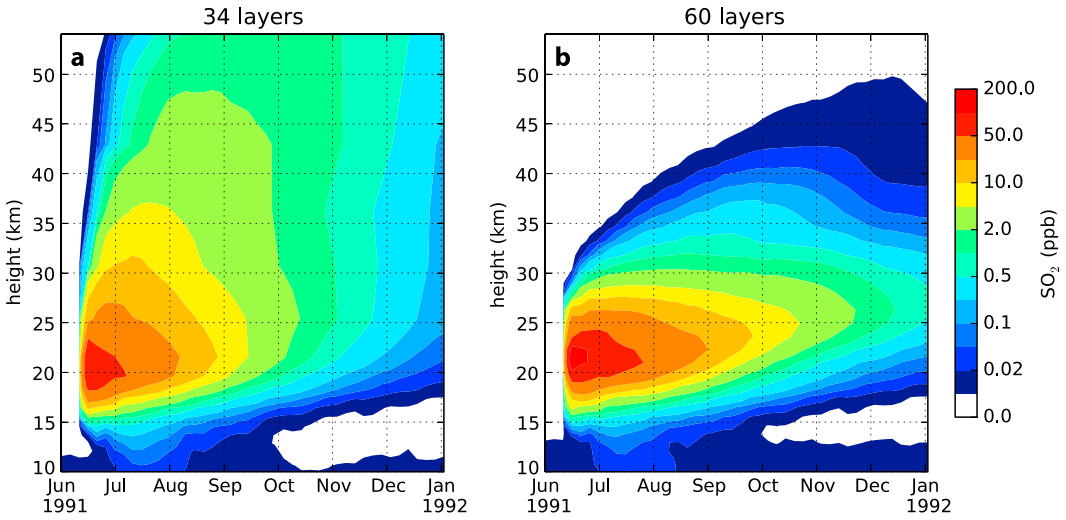

Figure A1. Mean SO_2 profile between 20°S and 20°N for (a) 34 layer and (b) 60 layer vertical resolution. Simulations with the 60 layer setup are discussed in the main text.

Appendix B: Emissions Setup

The emissions used in the model are as follows. Anthropogenic emissions of CH_4, CO, nitrogen oxides (NO_X), nonmethane volatile organic compounds (NMVOC), sulfur dioxide (SO_2), and ammonia (NH_3) were taken from the Emissions Database for Global Atmospheric Research (EDGAR) version 4.2 [*European Commission and Joint Research Centre (JRC)/Netherlands Environmental Assessment Agency (PBL)*, 2011], except for transport sectors. EDGAR version 4.1 was used for the transport sectors because it provides aircraft NO_X emissions separately and allows us to implement a different vertical distribution of these emissions compared to other transport related emissions. Since the vertical distribution of aircraft NO_X emissions is not included in EDGAR 4.1, we used the monthly three-dimensional historical aircraft emissions provided for the ACCMIP and the Coupled Model Intercomparison Project [*Lamarque et al.*, 2010]. These emissions were scaled with the global yearly aircraft NO_X emission total from EDGAR 4.1 to include a realistic interannual variability. For the yearly anthropogenic NMVOC emissions from EDGAR, VOC speciation was applied on a grid cell and sector basis according to the historical ACCMIP emissions for the year 2000. The anthropogenic EDGAR emissions for each species were scaled to match the total yearly anthropogenic emissions from the Regional Emission Inventory in Asia (REAS) version 1 [*Ohara et al.*, 2007] over the South and East Asian region, between 50°N and 10°S latitude and 60°E and 150°E longitude. Seasonal cycles for the EDGAR emissions were implemented following the recommendations of *Veldt* [1992]. Decadal anthropogenic emissions from the historical ACCMIP emission inventory were used for black carbon (BC) and organic carbon (OC), linearly interpolated to the simulation years.

Biomass burning emissions were used from the Reanalysis of the Tropospheric chemical composition over the past 40 years project (RETRO), inventory [*Schultz et al.*, 2008]. Production of NO_X by lightning and emissions of dimethyl sulfide (DMS) and sea salt are calculated online [*Huijnen et al.*, 2010; *Vignati et al.*, 2010]. Natural CH_4 monthly emissions were taken from the Hydrogen, Methane, And Nitrous Oxide project [*Spahni et al.*, 2011], including emissions and soil uptake from the LPJ-WhyMe vegetation model. Natural emissions of CO, NO_X, NH_3, and NMVOC were prescribed using a monthly data set from the Monitoring Atmospheric Composition and Climate (MACC) project, as in *van Noije et al.* [2014]. The emission heights of anthropogenic, biomass burning, and natural emissions have been revised, as described in *van Noije et al.* [2014].

Appendix C: Sensitivity to Injection Height

The injection height of the Pinatubo SO_2 is an important parameter for determining the plume evolution. The initial evolution of the erupted SO_2 is driven by reactions on volcanic ice and ash particles, and by dynamical changes due to absorption by sulfate and ash. Generally, not all of these processes are included in studies of the Pinatubo eruption, and the assumed SO_2 injection needs to account for missing processes. Therefore, the best injection height and the model sensitivity to this parameter might be dependent on the model setup. More studies are needed to quantify these parameters, preferably using climate models with radiatively interactive aerosols.

We test here two more injection height scenarios apart from the setup presented in the main text, where most SO_2 was injected between 17 and 21 km. In these additional simulations the SO_2 was injected between 15 and 27 km in scenario H1, and between 15 and 24 km in scenario H2. The bulk of the material (80%) was injected in the highest 4 km (23–27 km and 20–24 km).

Figure C1 shows the AOD evolution for the three scenarios in the year after the eruption. The middle-injection and high-injection heights give larger AOD values in the northern tropical region, which would deteriorate the comparison with SAGE II observations in this region. The transport of the aerosols to high latitudes and the Southern Hemisphere is also less well captured in these simulations. For the high scenario H1, most of the material is transported within the tropical pipe. This leads to reduced transport to high latitudes in the first 5 months after the eruption, most aerosol remaining confined in the northern tropical region. For both H1 and H2, the plume is dominantly transported to the Northern Hemisphere, and the AOD values in the northern midlatitudes are highly overestimated. Although the emission scenario in the main text also overestimates the AOD in the tropics and the high northern latitudes, the overestimate is smaller for this scenario, and the transport of the plume to both hemispheres is better captured. We chose

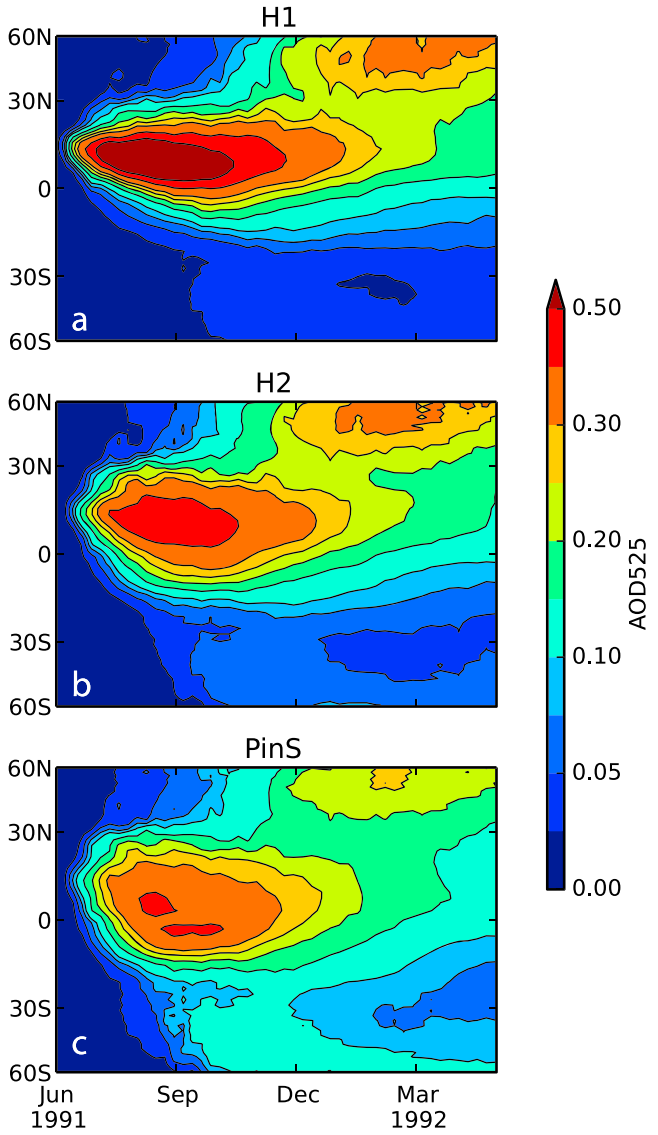

Figure C1. Zonal mean modeled AOD at 525 nm (AOD525) for three injection heights. The bulk of SO_2 emission was assumed between (a) 23–27 km for H1, (b) 20–24 km for H2, and (c) 17–23 km for the PinS simulation.

the low-injection scenario for the rest of the paper because it represents best the observed global aerosol distribution. In addition, the modeled peak aerosol backscatter values between 20 and 25 km altitude above Mauna Loa in July 1991 correspond best with lidar measurements (Figure 2).

Acknowledgments
This work was supported by the Netherlands Organisation for Scientific Research (NWO) and the EU FP7 Integrated Project PEGASOS. We thank SURFsara (www.surfsara.nl) for the support in using the Dutch national supercomputer Cartesius. We would like to thank the anonymous reviewers for their helpful and constructive comments. AVHRR data used in this study were obtained from NOAA's National Climatic Data Center (http://www.ncdc.noaa.gov). Model output presented in this paper is available upon request from the corresponding author.

References

Aan de Brugh, J. M. J. (2013), Aerosol processes relevant for the Netherlands, Wageningen Univ., Wageningen, Netherlands.

Aan de Brugh, J. M. J., M. Schaap, E. Vignati, F. Dentener, M. Kahnert, M. Sofiev, V. Huijnen, and M. C. Krol (2011), The European aerosol budget in 2006, *Atmos. Chem. Phys.*, *11*, 1117–1139, doi:10.5194/acp-11-1117-2011.

Andronova, N. G., E. V. Rozanov, F. Yang, M. E. Schlesinger, and G. L. Stenchikov (1999), Radiative forcing by volcanic aerosols from 1850 to 1994, *J. Geophys. Res.*, *104*(D14), 16,807–16,826, doi:10.1029/1999JD900165.

Ansmann, A., F. Wagner, U. Wandinger, I. Mattis, U. Gorsdorf, H.-D. Dier, and J. Reichardt (1996), Pinatubo aerosol and stratospheric ozone reduction: Observations over central Europe, *J. Geophys. Res.*, *101*(D13), 18,775–18,785.

Aquila, V., L. D. Oman, R. S. Stolarski, P. R. Colarco, and P. A. Newman (2012), Dispersion of the volcanic sulfate cloud from a Mount Pinatubo-like eruption, *J. Geophys. Res.*, *117*, D06216, doi:10.1029/2011JD016968.

Bândă, N., M. Krol, M. van Weele, T. van Noije, and T. Röckmann (2013), Analysis of global methane changes after the 1991 Pinatubo volcanic eruption, *Atmos. Chem. Phys.*, *13*(4), 2267–2281, doi:10.5194/acp-13-2267-2013.

Barnes, J. E., and D. J. Hofmann (1997), Lidar measurements of stratospheric aerosol over Mauna Loa observatory, *Geophys. Res. Lett.*, *24*(15), 1923–1926.

Bauman, J. J., P. B. Russell, and P. Hamill (2003), A stratospheric aerosol climatology from SAGE II and CLAES measurements: 2. Results and comparisons, 1984–1999, *J. Geophys. Res.*, *108*(D13), 4383, doi:10.1029/2002JD002993.

Bekki, S., and K. S. Law (1997), Sensitivity of the atmospheric CH_4 growth rate to global temperature changes observed from 1980 to 1992, *Tellus B*, *49*(4), 409–416.

Bekki, S., R. Toumi, and J. A. Pyle (1993), Role of sulphur photochemistry in tropical ozone changes after the eruption of Mount Pinatubo, *Nature*, *362*(6418), 331–333.

Bekki, S., K. S. Law, and J. A. Pyle (1994), Effect of ozone depletion on atmospheric CH_4 and CO concentrations, *Nature*, *371*, 595–597.

Bekki, S., J. A. Pyle, W. Zhong, R. Toumi, J. D. Haigh, and D. M. Pyle (1996), The role of microphysical and chemical processes in prolonging the climate forcing of the Toba Eruption, *Geophys. Res. Lett.*, *23*(19), 2669–2672, doi:10.1029/96GL02088.

Bogumil, K., et al. (2003), Measurements of molecular absorption spectra with the SCIAMACHY pre-flight model: Instrument characterization and reference data for atmospheric remote-sensing in the 230–2380 nm region, *J. Photochem. Photobiol. A*, *157*(2–3), 167–184, doi:10.1016/S1010-6030(03)00062-5.

Bousquet, P., D. A. Hauglustaine, P. Peylin, C. Carouge, and P. Ciais (2005), Two decades of OH variability as inferred by an inversion of atmospheric transport and chemistry of methyl chloroform, *Atmos. Chem. Phys.*, *5*, 2635–2656.

Bousquet, P., et al. (2006), Contribution of anthropogenic and natural sources to atmospheric methane variability, *Nature*, *443*(7110), 439–443, doi:10.1038/nature05132.

Burnett, C. R., and E. B. Burnett (1984), Observational results on the vertical column abundance of atmospheric hydroxyl: Description of its seasonal behavior 1977–1982 and of the 1982 El Chichon Perturbation, *J. Geophys. Res.*, *89*(D6), 9603–9611, doi:10.1029/JD089iD06p09603.

Carslaw, K. S., S. L. Clegg, and P. Brimblecombe (1995), A thermodynamic model of the system HCl-HNO3-H2SO4-H2O, including solubilities of HBr, from <200 to 328 K, *J. Phys. Chem.*, *99*, 11,557–11,574.

Dee, D. P., et al. (2011), The ERA-Interim reanalysis: Configuration and performance of the data assimilation system, *Q. J. R. Meteorol. Soc.*, *137*, 553–597, doi:10.1002/qj.828.

Denman, K., et al. (2007), Couplings between changes in the climate system and biogeochemistry, in *Climate Change 2007: The Physical Science Basis. Contribution of Working Group I to the Fourth Assessment Report of the Intergovernmental Panel on Climate Change*, edited by S. Solomon et al., Cambridge Univ. Press, Cambridge, U. K., and New York.

Deshler, T. (2008), A review of global stratospheric aerosol: Measurements, importance, life cycle, and local stratospheric aerosol, *Atmos. Res.*, *90*, 223–232, doi:10.1016/j.atmosres.2008.03.016.

Dhomse, S. S., et al. (2014), Aerosol microphysics simulations of the Mt. Pinatubo eruption with the UM-UKCA composition-climate model, *Atmos. Chem. Phys.*, *14*(20), 11,221–11,246, doi:10.5194/acp-14-11221-2014.

Dlugokencky, E. J., K. A. Masaire, P. M. Lang, P. P. Tans, L. P. Steele, and E. G. Nisbet (1994), A dramatic decrease in the growth rate of atmospheric methane in the Northern Hemisphere during 1992, *Geophys. Res. Lett.*, *21*(1), 45–48.

Dlugokencky, E. J., E. G. Dutton, P. C. Novelli, P. P. Tans, K. A. Masarie, K. O. Lantz, and S. Madronich (1996), Changes in CH_4 and CO growth rates after the eruption of Mt. Pinatubo and their link with changes in tropical tropospheric UV flux, *Geophys. Res. Lett.*, *23*(20), 2761–2764.

Doiron, S. D., G. J. S. Bluth, C. C. Schnetzler, A. J. Krueger, and L. S. Walter (1991), Transport of Cerro Hudson SO_2 clouds, *Eos Trans. AGU*, *72*(45), 489–498, doi:10.1029/90EO00354.

Dutton, E. G., and J. R. Christy (1992), Solar radiative forcing at selected locations and evidence for global lower tropospheric cooling following the eruptions of El Chichón and Pinatubo, *Geophys. Res. Lett.*, *19*(23), 2313–2316, doi:10.1029/92GL02495.

English, J. M., O. B. Toon, and M. J. Mills (2013), Microphysical simulations of large volcanic eruptions: Pinatubo and Toba, *J. Geophys. Res. Atmos.*, *118*, 1880–1895, doi:10.1002/jgrd.50196.

European Commission, and Joint Research Centre (JRC)/Netherlands Environmental Assessment Agency (PBL) (2011), Emission Database for Global Atmospheric Research (EDGAR), release version 4.1 and 4.2.

Fuglestvedt, J. S., J. E. Johnson, and I. S. A. Isaksen (1994), Effects of reductions in stratospheric ozone on tropospheric chemistry through changes in photolysis rates, *Tellus B*, *46*, 172–192.

GLOBALVIEW-CH4 (2009), *Cooperative Atmospheric Data Integration Project—Methane* [CD-ROM], NOAA ESRL, Boulder, Colo. [Also available on Internet via anonymous FTP to ftp://ftp.cmdl.noaa.gov,Path:ccg/ch4/GLOBALVIEW.]

Grooß, J.-U., and J. Russell III (2005), Technical note: A stratospheric climatology for O_3, H_2O, CH_4, NO_x, HCl and HF derived from HALOE measurements, *Atmos. Chem. Phys.*, *5*, 2797–2807.

Guo, S., G. J. S. Bluth, W. I. Rose, I. M. Watson, and A. J. Prata (2004), Re-evaluation of SO_2 release of the 15 June 1991 Pinatubo eruption using ultraviolet and infrared satellite sensors, *Geochem. Geophys. Geosyst.*, *5*, Q04001, doi:10.1029/2003GC000654.

Houweling, S., F. Dentener, and J. Lelieveld (1998), The impact of nonmethane hydrocarbon compounds on tropospheric photochemistry radical, *J. Geophys. Res.*, *103*(D9), 10,673–10,696.

Huijnen, V., et al. (2010), The global chemistry transport model TM5: description and evaluation of the tropospheric chemistry version 3.0, *Geosci. Model Dev.*, *3*, 445–473, doi:10.5194/gmd-3-445-2010.

Kirschke, S., et al. (2013), Three decades of global methane sources and sinks, *Nat. Geosci.*, *6*(10), 813–823, doi:10.1038/ngeo1955.

Kokkola, H., R. Hommel, J. Kazil, U. Niemeier, A.-I. Partanen, J. Feichter, and C. Timmreck (2009), Aerosol microphysics modules in the framework of the ECHAM5 climate model-intercomparison under stratospheric conditions, *Geosci. Model Dev.*, *2*(2), 97–112, doi:10.5194/gmd-2-97-2009.

Krol, M., and J. Lelieveld (2003), Can the variability in tropospheric OH be deduced from measurements of 1,1,1-trichloroethane (methyl chloroform)?, *J. Geophys. Res.*, *108*(D3), 4125, doi:10.1029/2002JD002423.

Lamarque, J.-F., et al. (2010), Historical (1850–2000) gridded anthropogenic and biomass burning emissions of reactive gases and aerosols: Methodology and application, *Atmos. Chem. Phys.*, *10*(15), 7017–7039, doi:10.5194/acp-10-7017-2010.

Lawrence, M. G., P. Joeckel, and R. von Kuhlmann (2001), What does the global mean OH concentration tell us?, *Atmos. Chem. Phys.*, *1*, 37–49.

Lelieveld, J., W. Peters, F. J. Dentener, and M. C. Krol (2002), Stability of tropospheric hydroxyl chemistry, *J. Geophys. Res.*, *107*(D23), 4715, doi:10.1029/2002JD002272.

Levy, H. (1971), Normal atmosphere: Large radical and formaldehyde concentrations predicted, *Science*, *173*(3992), 141–143, doi:10.1126/science.173.3992.141.

Long, C. S., and L. L. Stowe (1994), Using the noaa/avhrr to study stratospheric aerosol optical thicknesses following the Mt. Pinatubo eruption, *Geophys. Res. Lett.*, *21*(20), 2215–2218, doi:10.1029/94GL01322.

Metzger, S., F. Dentener, S. Pandis, and J. Lelieveld (2002), Gas/aerosol partitioning: 1. A computationally efficient model, *J. Geophys. Res.*, *107*(D16), ACH 16-1–ACH 16-24, doi:10.1029/2001JD001102.

Monteil, G., S. Houweling, E. J. Dlugockenky, G. Maenhout, B. H. Vaughn, J. W. C. White, and T. Rockmann (2011), Interpreting methane variations in the past two decades using measurements of CH_4 mixing ratio and isotopic composition, *Atmos. Chem. Phys.*, *11*, 9141–9153, doi:10.5194/acp-11-9141-2011.

Montzka, S. A., E. J. Dlugokencky, and J. H. Butler (2011), Non-CO_2 greenhouse gases and climate change, *Nature*, *476*, 43–50, doi:10.1038/nature10322.

Nagai, T., B. Liley, T. Sakai, T. Shibata, and O. Uchino (2010), Post-pinatubo evolution and subsequent trend of the stratospheric aerosol layer observed by mid-latitude lidars in both hemispheres, *SOLA*, *6*, 69–72, doi:10.2151/sola.2010-018.

Naik, V., et al. (2013), Preindustrial to present-day changes in tropospheric hydroxyl radical and methane lifetime from the Atmospheric Chemistry and Climate Model Intercomparison Project (ACCMIP), *Atmos. Chem. Phys.*, *13*(10), 5277–5298, doi:10.5194/acp-13-5277-2013.

Niemeier, U., C. Timmreck, H.-F. Graf, S. Kinne, S. Rast, and S. Self (2009), Initial fate of fine ash and sulfur from large volcanic eruptions, *Atmos. Chem. Phys.*, *9*, 9043–9057.

Ohara, T., H. Akimoto, J. Kurokawa, N. Horii, K. Yamaji, X. Yan, and T. Hayasaka (2007), An Asian emission inventory of anthropogenic emission sources for the period 1980–2020, *Atmos. Chem. Phys.*, *7*(16), 4419–4444, doi:10.5194/acp-7-4419-2007.

Oikonomou, E. K., and A. O'Neill (2006), Evaluation of ozone and water vapor fields from the ECMWF reanalysis ERA-40 during 1991–1999 in comparison with UARS satellite and MOZAIC aircraft observations, *J. Geophys. Res.*, *111*, D14109, doi:10.1029/2004JD005341.

Prather, M. J. (1986), Numerical advection by conservation of second-order moments, *J. Geophys. Res.*, *91*(D6), 6671–6681, doi:10.1029/JD091iD06p06671.

Prather, M. J., C. D. Holmes, and J. Hsu (2012), Reactive greenhouse gas scenarios: Systematic exploration of uncertainties and the role of atmospheric chemistry, *Geophys. Res. Lett.*, *39*, L09803, doi:10.1029/2012GL051440.

Prinn, R. G., et al. (2005), Evidence for variability of atmospheric hydroxyl radicals over the past quarter century, *Geophys. Res. Lett.*, *32*, L07809, doi:10.1029/2004GL022228.

Read, W., L. Froidevaux, and J. W. Waters (1993), Microwave limb sounder measurement of stratospheric SO_2 from the Mt. Pinatubo volcano, *Geophys. Res. Lett.*, *20*(12), 1299–1302.

Russell, G. L., and J. A. Lerner (1981), A new finite-differencing scheme for the tracer transport equation, *J. Appl. Meteorol.*, *20*(12), 1483–1498, doi:10.1175/1520-0450(1981)020<1483:ANFDSF>2.0.CO;2.

Schultz, M. G., A. Heil, J. J. Hoelzemann, A. Spessa, K. Thonicke, J. G. Goldammer, A. C. Held, J. M. C. Pereira, and M. van het Bolscher (2008), Global wildland fire emissions from 1960 to 2000, *Global Biogeochem. Cycles*, *22*, GB2002, doi:10.1029/2007GB003031.

Spahni, R., et al. (2011), Constraining global methane emissions and uptake by ecosystems, *Biogeosciences*, *8*, 1643–1665, doi:10.5194/bg-8-1643-2011.

Stratospheric Processes and their Role in Climate (SPARC): Assessment of Stratospheric Aerosol Properties (ASAP) (2006), *SPARC Rep. 4, WCRP-124, WMO- 1295,* edited by L. Thomason and T. Peter.

Stenchikov, G. L., I. Kirchner, A. Robock, H.-F. Graf, J. C. Antuña, R. G. Grainger, A. Lambert, and L. Thomason (1998), Radiative forcing from the 1991 Mount Pinatubo volcanic eruption, *J. Geophys. Res.*, *103*(D12), 13,837–13,857, doi:10.1029/98JD00693.

Telford, P., P. Braesicke, O. Morgenstern, and J. Pyle (2009), Reassessment of causes of ozone column variability following the eruption of Mount Pinatubo using a nudged CCM, *Atmos. Chem. Phys. Discuss.*, *9*(2), 5423–5446, doi:10.5194/acpd-9-5423-2009.

Thomason, L. W., S. P. Burton, B.-P. Luo, and T. Peter (2008), SAGE II measurements of stratospheric aerosol properties at non-volcanic levels, *Atmos. Chem. Phys.*, *8*, 983–995.

Timmreck, C., and H.-F. Graf (2006), The initial dispersal and radiative forcing of a Northern Hemisphere mid-latitude super volcano: A model study, *Atmos. Chem. Phys.*, *6*(1), 35–49, doi:10.5194/acp-6-35-2006.

Timmreck, C., H.-F. Graf, and I. Kirchner (1999), A one and half year interactive MA/ECHAM4 simulation of Mount Pinatubo aerosol, *J. Geophys. Res.*, *104*(D8), 9337–9359, doi:10.1029/1999JD900088.

Toohey, M., K. Krüger, U. Niemeier, and C. Timmreck (2011), The influence of eruption season on the global aerosol evolution and radiative impact of tropical volcanic eruptions, *Atmos. Chem. Phys.*, *11*(23), 12,351–12,367, doi:10.5194/acp-11-12351-2011.

van der A, R. J., M. A. F. Allaart, and H. J. Eskes (2010), Multi sensor reanalysis of total ozone, *Atmos. Chem. Phys.*, *10*(22), 11,277–11,294, doi:10.5194/acp-10-11277-2010.

van Noije, T. P. C., P. Le Sager, A. Segers, P. F. J. van Velthoven, M. C. Krol, and W. Hazeleger (2014), Simulation of tropospheric chemistry and aerosols with the climate model EC-Earth, *Geosci. Model Dev. Discuss.*, *7*, 1933–2006, doi:10.5194/gmdd-7-1933-2014.

Veldt, C. (1992), Updating and upgrading the PHOXA emission database to 1990, *Tech. Rep. TNO report R 92-118/112322-23155*, TNO-MW, Delft, Netherlands.

Vignati, E., J. Wilson, and P. Stier (2004), M7: An efficient size-resolved aerosol microphysics module for large-scale aerosol transport models, *J. Geophys. Res.*, *109*, D22202, doi:10.1029/2003JD004485.

Vignati, E., M. Facchini, M. Rinaldi, C. Scannell, D. Ceburnis, J. Sciare, M. Kanakidou, S. Myriokefalitakis, F. Dentener, and C. O'Dowd (2010), Global scale emission and distribution of sea-spray aerosol: Sea-salt and organic enrichment, *Atmos. Environ.*, *44*(5), 670–677, doi:10.1016/j.atmosenv.2009.11.013.

Voulgarakis, A., et al. (2013), Analysis of present day and future OH and methane lifetime in the ACCMIP simulations, *Atmos. Chem. Phys.*, *13*(5), 2563–2587, doi:10.5194/acp-13-2563-2013.

Walter, B. P., M. Heimann, and E. Matthews (2001), Modeling modern methane emissions from natural wetlands 2. Interannual variations 1982–1993, *J. Geophys. Res.*, *106*(D24), 34,207–34,219.

Wang, J. S., J. A. Logan, M. B. Mcelroy, B. N. Duncan, I. A. Megretskaia, and R. M. Yantosca (2004), A 3-D model analysis of the slowdown and interannual variability in the methane growth rate from 1988 to 1997, *Global Biogeochem. Cycles*, *18*, GB3011, doi:10.1029/2003GB002180.

Williams, J. E., J. Landgraf, A. Bregman, and H. H. Walter (2006), A modified band approach for the accurate calculation of online photolysis rates in stratospheric-tropospheric chemical transport models, *Atmos. Chem. Phys.*, *6*, 4137–4161.

Williams, J. E., A. Strunk, V. Huijnen, and M. van Weele (2012), The application of the modified band approach for the calculation of on-line photodissociation rate constants in TM5: Implications for oxidative capacity, *Geosci. Model Dev.*, *5*, 15–35, doi:10.5194/gmd-5-15-2012.

Wolfe, E. W., and R. P. Hoblitt (1996), Overview of the Eruptions, in *FIRE and MUD: Eruptions and Lahars of Mount Pinatubo, Philippines*, edited by C. G. Newhall and R. S. Punongbayan, pp. 3–20, Univ. of Washington Press and Phil. Inst. of Volcanol. and Seismolog., Seattle, Wash., and Quezon City, Philippines.

Young, R. E., H. Houben, and O. B. Toon (1994), Radiatively forced dispersion of the Mt. Pinatubo volcanic cloud and induced temperature perturbations in the stratosphere during the first few months following the eruption, *Geophys. Res. Lett.*, *21*(5), 367–372.
Zeleznik, F. J. (1991), Thermodynamic properties of the aqueous sulfuric acid systems to 350 K, *J. Phys. Chem. Ref. Data*, *20*(6), 1157–1198.
Zhao, T. X.-P., P. K. Chan, and A. K. Heidinger (2013), A global survey of the effect of cloud contamination on the aerosol optical thickness and its long-term trend derived from operational AVHRR satellite observations, *J. Geophys. Res. Atmos.*, *118*, 2849–2857, doi:10.1002/jgrd.50278.